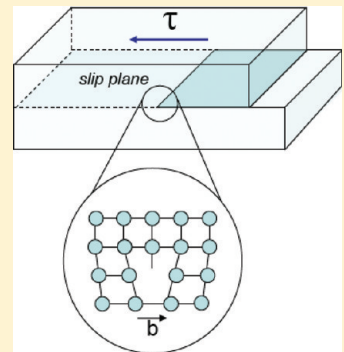


Large Amplitude Oscillatory Shear of Block Copolymer Spheres on a Body-Centered Cubic Lattice: Are Micelles Like Metals?

Maria A. Torija,[†] Soo-Hyung Choi,[‡] Timothy P. Lodge,^{*,‡,§} and Frank S. Bates^{*,‡}

[†]CSE Characterization Facility, [‡]Department of Chemical Engineering & Materials Science, and [§]Department of Chemistry, University of Minnesota, Minneapolis, Minnesota 55455, United States

ABSTRACT: Small-angle X-ray diffraction experiments have uncovered a remarkable mechanism of grain alignment during plastic deformation of ordered sphere-forming diblock copolymer micelles when subjected to large amplitude dynamic shearing. A nearly monodisperse poly(styrene-*b*-ethylene-*alt*-propylene) (SEP) diblock copolymer with block molecular weights of 42 000 and 60 000 was mixed with squalane ($C_{30}H_{62}$), an EP selective solvent, at a concentration of 10 wt %. After high temperature annealing, the sample formed an ordered polydomain morphology containing glassy S cores at room temperature. SAXS powder patterns confirm body-centered cubic (BCC) symmetry and reveal the development of a complex array of two-dimensionally resolved Bragg reflections following the application, and cessation, of oscillatory shearing. These diffraction results are interpreted on the basis of the classic mechanism of crystalline slip, which accounts for plastic deformation of ductile materials such as metals. Four distinct slip systems are shown to be active in this work, suggesting a robust basis for deforming and mixing of soft ordered solids.



I. INTRODUCTION

The response of ordered materials to applied stresses dictates the processing strategies and product applications of many forms of condensed matter. Brittle materials, such as silicon and diamond, fracture prior to yielding due to the inability of the underlying covalent bonds and crystalline lattice to support the generation and movement of dislocations. Ductile compounds, best exemplified by metals like copper and gold and engineering alloys such as steel, plastically deform when loaded beyond the yield stress. These hard materials typically fail at engineering strains $0.02 < \varepsilon < 0.5$, where $\varepsilon = (l - l_0)/l_0$, and l_0 and l represent the initial and loaded length of a specimen in tension, respectively. Because the yield strain for most metals and alloys is generally quite small, $\varepsilon_y < 0.02$, nearly all of the extension is accounted for by plasticity, which can be directly correlated with mechanical toughness.

Application of a tensile force to an ordered specimen produces shear stresses that depend on the crystal symmetry and the unit cell orientation. Certain combinations of planes and directions known as slip systems, referred to as $(hkl)[\bar{h}'k'l']$, are particularly susceptible to producing irreversible motion between planes, that is, coherent movement of one plane of atoms relative to the adjacent plane of atoms. Such displacements can be facilitated by the movement of line defects known as dislocations along specific crystallographic planes (hkl) in a direction $[\bar{h}'k'l']$ that minimizes the magnitude of each hopping step, where h , k , and l are Miller indices.^{1,2} Figure 1 illustrates the structure of an edge dislocation and identifies the geometry associated with the slip plane and slip direction defined by the Burgers vector b .

High symmetry crystals contain multiple slip systems that combine families of slip planes $\{hkl\}$ and slip directions $\langle h'k'l' \rangle$. For body-centered cubic (BCC) materials, the most accessible slip systems are $\{110\}\langle\bar{1}11\rangle$, $\{211\}\langle\bar{1}11\rangle$, and $\{321\}\langle\bar{1}11\rangle$,

totaling 48 discrete combinations.² In each case, the slip direction is coincident with the closest linear packing of spheres along the body diagonal of the unit cell, which minimizes the displacement $b = |b|$ required to accommodate dislocation movement. Sketches of these three familiar slip systems, along with the fourth in the series, $\{431\}\langle\bar{1}11\rangle$ (discussed below), are provided in Figure 2.

Application of a tensile stress (σ) to a material produces resolved shear stresses, $\tau_R = \sigma \cos \phi \cos \lambda$, determined by the angles ϕ and λ formed between the direction of the applied force and the normal to the slip plane and the slip direction, respectively.² Because one or more of the 48 (or more) slip systems inevitably satisfies the condition $\phi \approx \lambda \approx 45^\circ$ in a BCC metal, the critical resolved shear stress τ_c required to induce slip is correlated in a simple manner with the yield stress in tension, $\sigma_y \approx 2\tau_c$. When a ductile polycrystalline metal (e.g., chromium or sodium) is stressed beyond σ_y , dislocations move along activated slip systems resulting in plastic deformation while preserving the overall morphology, for example, the grain texture.

Plastic deformation in soft ordered solids has not been investigated to the same extent as hard crystalline materials. Block copolymers present attractive opportunities in this regard, both in the bulk melt state and when mixed with low molecular weight solvents. This class of materials offers an opportunity to manipulate the geometry of the microdomain morphology (e.g., spheres versus cylinders) as well as the state of long-range order.³ In this Article, we consider one of the simplest cases: a sphere-forming diblock copolymer mixed with a selective solvent that leads to a BCC ordering of micelles. Shear-induced structuring of ordered block copolymer melts and solutions has been the

Received: March 15, 2011

Published: April 27, 2011

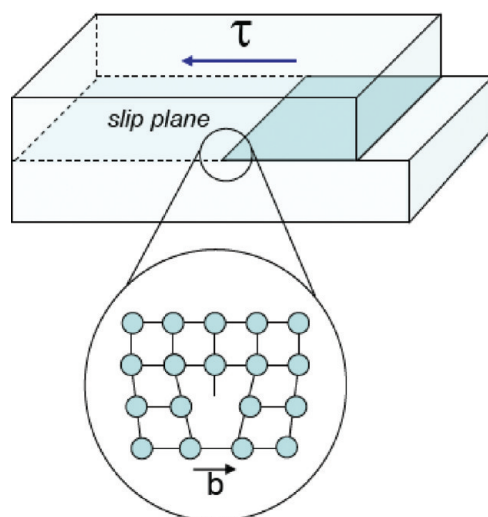


Figure 1. Shear stress (τ)-induced generation of an edge dislocation in a crystalline material, where b represents the Burgers vector.

subject of intense study for many years beginning with the seminal work of Keller and Odell on cylinder alignment.⁴ Several groups have examined the effect of shear on BCC copolymer micelles, both in solution and in the melt. These studies include both diblocks and triblocks, as well as oscillatory and steady flow.^{5–19}

In previous publications, we have reported on the structure²⁰ and molecular exchange dynamics^{21,22} of poly(styrene-*b*-ethylene-*alt*-propylene) (SEP) diblock copolymers mixed with the model organic solvent squalane ($C_{30}H_{62}$) at concentrations ranging from 0.5% to 15% by weight polymer. Squalane is a selective solvent for the EP block, resulting in the self-assembly of spherical micelles containing a polystyrene core when $f_S < 0.5$, where f_S represents the volume fraction of S in the diblock copolymer. At low polymer concentrations (below about 5–7% by weight, depending on the overall molecular weight), the SEP micelles are disordered, leading to liquid-like behavior and a relatively low viscosity. Increasing the diblock copolymer concentration above the order-disorder concentration (ODC) results in the formation of BCC crystals, evidenced both by a distinctive diffraction pattern in small-angle X-ray scattering (SAXS) experiments and by a solid-like viscoelastic response including a frequency-independent linear dynamic elastic modulus, $G' \approx \omega^0$. Recently, we have demonstrated that deuterium labeled micelles that assemble into BCC crystals (15% by weight dSEP) can be thoroughly mixed with the normal counterpart (*h*SEP) using a simple laboratory scale mixing device.²³ This finding raises an intriguing question: How do such soft solids accommodate large scale deformation (e.g., a shearing flow), and how does the associated mechanism result in statistically uniform blending down to the smallest material dimensions, that is, the micelle diameter?

Two limiting hypotheses can be advanced. In one extreme, the application of shear at a sufficiently high rate may disorder (i.e., melt) the crystals, facilitating intermixing of the labeled and unlabeled micelles. Shear-induced melting has been documented in several instances at large imposed stresses (or strains).^{9,13–15,19} Alternatively, activation of various slip systems, as occurs in ductile hard materials,^{1,2} may induce massive plastic deformation, and possibly disruption of crystalline grains, without actually melting the entire ordered structure. The signature of each mechanism is expected to be different, with the former leading to strictly powder

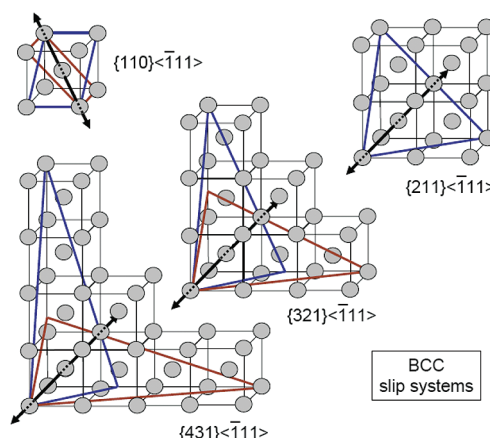


Figure 2. Four slip systems associated with dislocation movement in BCC crystalline materials. Twin slip planes are identified by the blue and red planes, and the common $\langle\bar{1}\bar{1}\bar{1}\rangle$ slip direction is delineated by the double ended arrows. The $\{110\}\langle\bar{1}\bar{1}\bar{1}\rangle$, $\{211\}\langle\bar{1}\bar{1}\bar{1}\rangle$, and $\{321\}\langle\bar{1}\bar{1}\bar{1}\rangle$ slip systems are commonly activated during the plastic deformation of BCC metals. Evidence of all four systems is found in the BCC ordered block copolymer micelle material described in this work.

diffraction, while the latter should produce resolvable features of single crystal diffraction. Indeed, in several instances, various preferred orientations of BCC crystals have been detected by small-angle scattering, depending on sample and flow history.^{9,11,17,19} We have designed these experiments to shed light on the actual deformation behavior of these weakly ordered soft solids (i.e., near the ODC) during large amplitude (50% strain amplitude) oscillatory shearing.

Here, we describe how a soft polycrystalline BCC material, formed from 10% SEP in squalane, responds to nonlinear dynamic shearing at 70 °C. SAXS patterns obtained upon cessation of flow reveal a rich assortment of two-dimensionally resolved diffraction spots, which can all be assigned to one of the four distinct slip systems shown in Figure 2. These results indicate that large amplitude oscillatory shearing of relatively dilute yet BCC ordered diblock copolymer micelles simultaneously induces long-range translational order while preserving a polydomain morphology, consistent with a classical mechanism of plastic deformation mediated by dislocation movement, rather than wholesale slipping of neighboring planes of spheres.

II. EXPERIMENTAL SECTION

An SEP diblock copolymer was prepared by selective hydrogenation of a poly(styrene-*b*-isoprene) precursor, which was synthesized by the sequential anionic polymerization of styrene and isoprene; a detailed description of the synthetic procedures is described elsewhere.²⁰ The polymers were characterized by size exclusion chromatography and 1H nuclear magnetic resonance spectroscopy to determine the overall molecular weight ($M_n = 102\,000$ g/mol), the overall composition (41% by mass PS), and polydispersity ($M_w/M_n = 1.05$). This polymer is referred to as SEP(42–60). Solutions of 10% by weight SEP(42–60) in squalane (Aldrich) were prepared gravimetrically using methylene chloride as a cosolvent; both diluents were used as received. The cosolvent was removed at room temperature under vacuum until constant weight was achieved.

Small-angle X-ray scattering was performed with the equipment maintained by the DuPont–Northwestern–Dow Collaborative

Access Team (DND-CAT) at the Advanced Photon Source, Argonne National Laboratory. Radiation of 17 keV, corresponding to a wavelength $\lambda = 0.7293 \text{ \AA}$, and a sample-to-distance of 0.656 m allowed access to a q range of $0.02 \text{ \AA}^{-1} \leq q \leq 0.12 \text{ \AA}^{-1}$, where q is the scattering wave vector defined as $q = 4\pi\lambda^{-1} \sin(\theta/2)$. For shearing specimens *in situ*, a DMTA rheometer (Rheometric Scientific) was installed on the beamline.²⁴ Specimens were placed between the two shear plates with sandwich geometry and covered with Kapton tape (ca. 50 μm thick). The sample was mounted such that the shearing direction is vertical, and the shear gradient axis is parallel to the X-ray beam (see Figure 3). Various frequencies (ω) between 1 and 500 rad/s and strain amplitudes (γ_0) between 1% and 60% were employed, although we restrict our attention in this Article to *in situ* measurements made at $\omega = 100 \text{ rad/s}$ with $\gamma_0 = 50\%$. The temperature was controlled by a ceramic heater maintained under a steady flow of helium. Additional rheological measurements were taken off-line using a parallel plate rheometer (TA Instruments Rheometrics Series ARES).

III. RESULTS AND ANALYSIS

A SAXS experiment conducted with the SEP(42–60)/squalane mixture prior to the application of oscillatory shearing

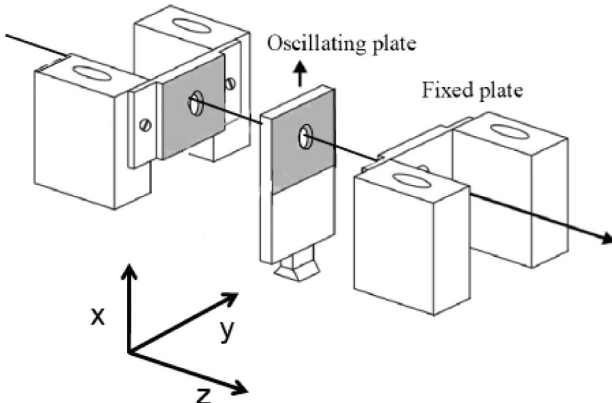


Figure 3. Schematic of the apparatus employed to conduct simultaneous oscillatory shearing and small-angle X-ray scattering on the ordered block copolymer micelles. The shear direction and shear plane correspond to x and $x-y$, respectively. The specimen is contained by Kapton windows (not shown), which are transparent to the X-ray beam.

produced a two-dimensional scattering pattern containing concentric rings of intensity as shown in Figure 4a. Careful examination of this powder pattern reveals numerous discrete spots within each diffraction ring, indicative of an underlying morphology that contains sizable single crystal grains. An azimuthally

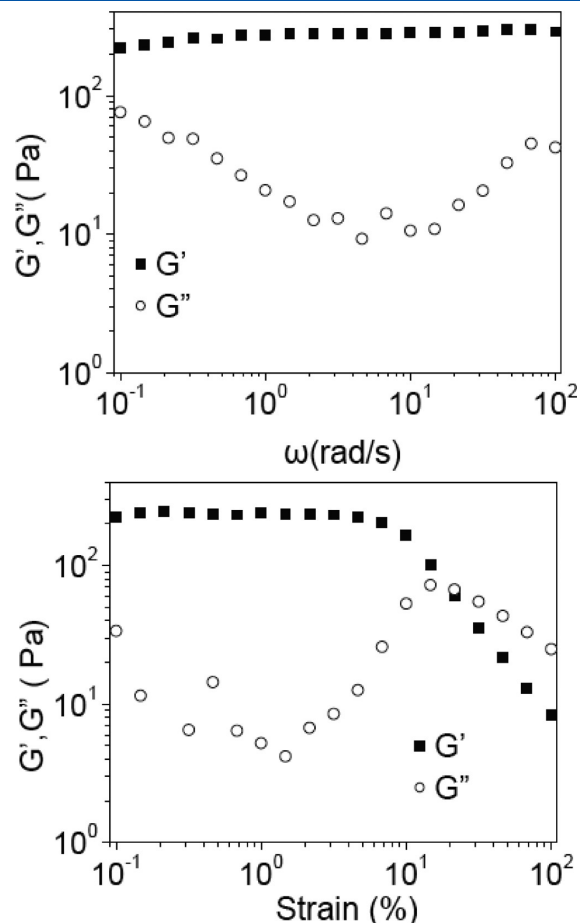


Figure 5. Dynamic elastic (G') and loss (G'') moduli obtained from the ordered SEP(42–60)/squalane mixture as a function of frequency (upper plot, $\gamma_0 = 1\%$) and strain amplitude ($\omega = 1 \text{ rad/s}$) at 70°C . The nonlinear viscoelastic behavior when $\gamma_0 > 5\%$ is associated with plastic deformation of the ordered BCC ordered structure.

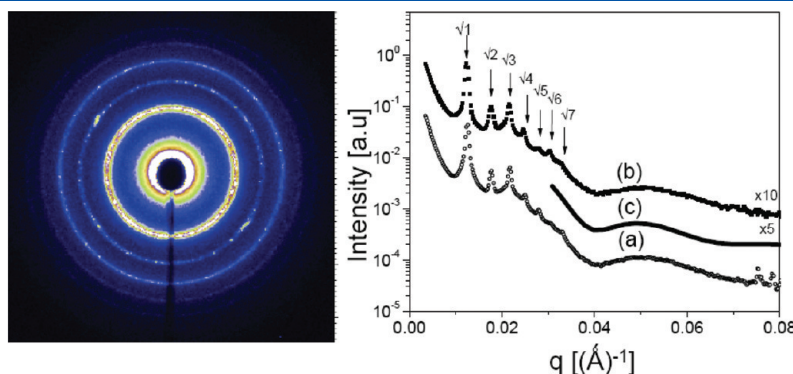


Figure 4. Two-dimensional SAXS pattern obtained from a mixture of 10% by weight SEP(42–60) in squalane at 70°C (left panel) prior to the application of large amplitude shearing. Azimuthal averaging to the one-dimensional form factor scattering (a) reveals at least seven diffraction peaks and distinctive form factor scattering consistent with the ordering of spherical micelles on a BCC lattice. The form factor scattering is modeled in (b) based on a poly(styrene) core radius $R_c = 11 \text{ nm}$ with a Gaussian spread of $\sigma_R = 0.4 \text{ nm}$. Virtually the same one-dimensional scattering pattern is obtained after dynamic shearing (c) (see Figure 6).

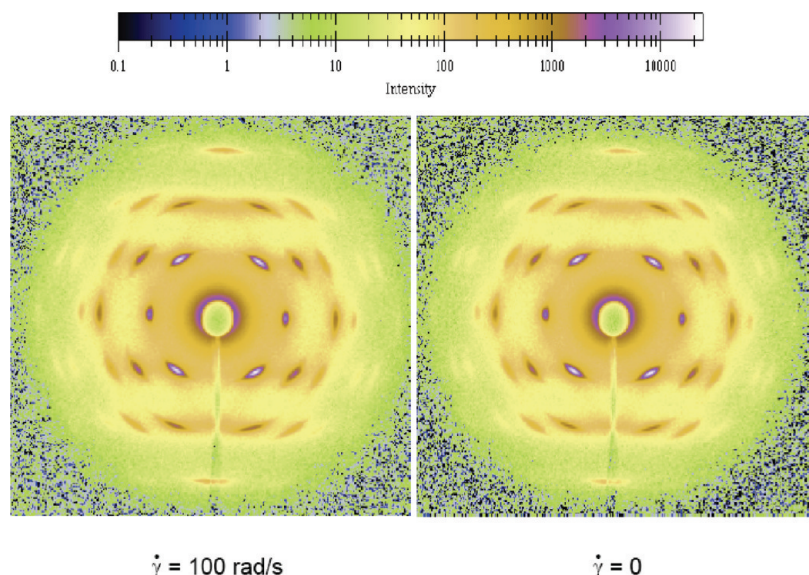


Figure 6. Two-dimensional SAXS patterns recorded during (left panel) and following (right panel) large amplitude ($\gamma_0 = 50\%$) oscillatory shearing of SEP(42–60) in squalane at 70 °C.

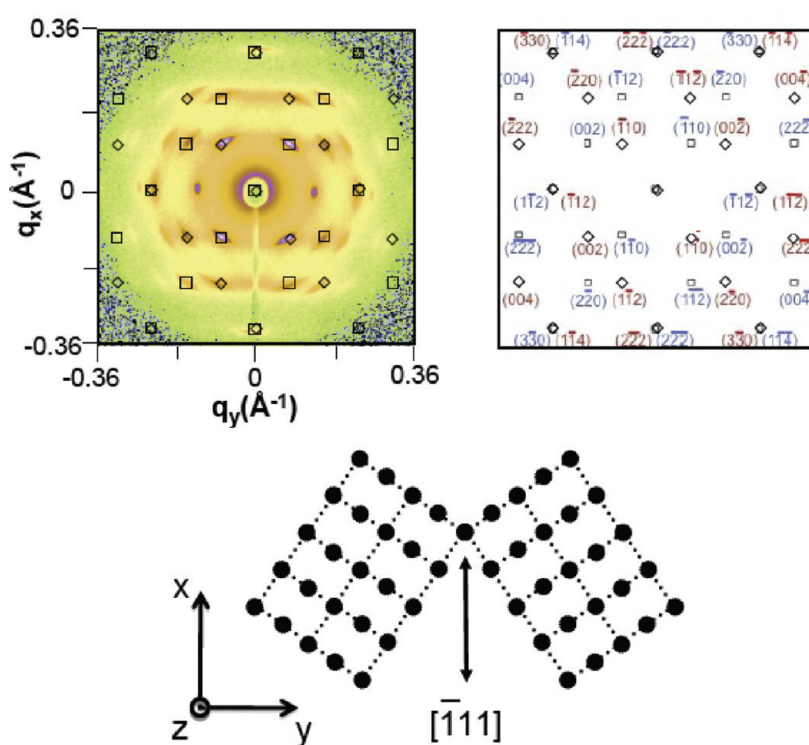


Figure 7. Identification of diffraction peaks associated with the $\{110\}\langle T11\rangle$ slip system, where the slip plane is parallel to the plane of shear ($x-y$) and the slip direction coincides with the shear direction (x). Equivalent twinned crystal structures are shown in the projection, and the associated reflections are located on the SAXS pattern using square and triangular symbols and indexed in the complementary map.

averaged one-dimensional version of this result, plotted in Figure 4b as intensity versus scattering wavevector q , produces at least seven distinct Bragg peaks with relative spacing $q/q^* = \sqrt{1}, \sqrt{2}, \sqrt{3}, \sqrt{4}, \sqrt{5}, \sqrt{6}, \sqrt{7}$, etc., where $q^* = 0.0125 \text{ \AA}^{-1}$, consistent with BCC symmetry and a unit cell parameter $a = 71 \text{ nm}$. The broad maximum in this SAXS pattern peaking at $q = 0.05 \text{ \AA}^{-1}$ derives from intraparticle (form factor) scattering from the spherical polystyrene cores. We have modeled this portion of the

data (solid curve) using a procedure described earlier,²⁰ yielding a core radius $R_c = 11.0 \text{ nm}$ with a Gaussian spread of $\sigma_R = 0.4 \text{ nm}$, nearly identical to the values reported previously.

Representative dynamic mechanical spectroscopy results, collected during linear isothermal frequency and isochronal strain sweep experiments, are presented in Figure 5. The ordered SEP-(42–60)/squalane mixture is clearly a soft elastic solid at 70 °C as evidenced by a frequency-independent dynamic elastic modulus,

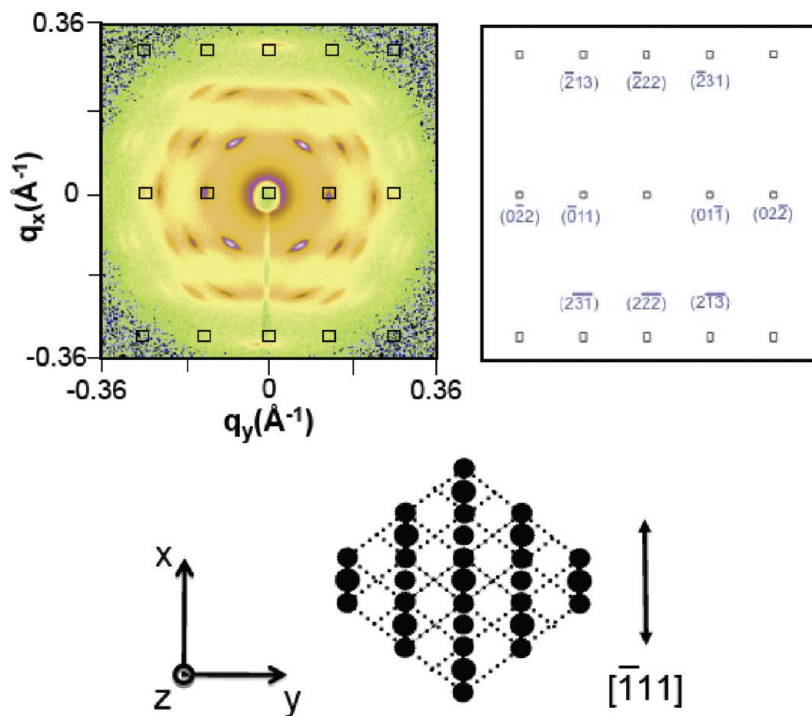


Figure 8. Identification of diffraction peaks associated with the $\{211\}\langle\bar{1}11\rangle$ slip system, where the slip plane is parallel to the plane of shear ($x-y$) and the slip direction coincides with the shear direction (x). Reflections associated with the projected view of the oriented crystal structure are located on the SAXS pattern using square symbols and indexed in the complementary map.

$G' \approx (2-3) \times 10^2 \text{ Pa}$,²⁵ determined with $\gamma_o = 1\%$. G' is nearly independent of strain amplitude (i.e., the elastic stress is linear in strain) up to $\gamma_o \approx 10\%$ (measured at 1 rad/s), while above this threshold the elastic modulus decreases rapidly with increasing γ_o , crossing below a rising dynamic loss modulus, G'' , at $\gamma_o = 20\%$.

Oscillatory shearing in the large strain amplitude (nonlinear) regime ($\gamma_o > 10\%$) leads to permanent changes to the SAXS pattern, as shown in Figure 6 for $\gamma_o = 50\%$ and $\omega = 100 \text{ rad/s}$. (We have made extensive measurements with ω and γ_o as variables, discussion of which will be deferred to a future publication. However, the prior work of Mortensen et al. should be noted in this regard;¹⁷ they have presented an appealing strain amplitude/frequency map of the response of triblock copolymer gels to oscillatory shear.) Two-dimensional scattering patterns were recorded while shearing, and again after cessation of shearing, following 3 min of oscillation (about 286 cycles). The original powder pattern has been converted to a complex array of diffraction spots indicative of well-defined crystalline order. However, we are not able to account for the spatial distribution of these reflections using a single crystal model, although reduction of the two-dimensional pattern to the one-dimensional form of intensity versus q confirms retention of BCC symmetry (see Figure 4).

We have determined that all of the diffraction spots evident in Figure 6 can be accounted for on the basis of the slip systems sketched in Figure 2, where the slip direction $\langle\bar{1}11\rangle$ is coincident with the direction of shear (x direction in Figure 3), and the four different slip planes are each oriented parallel to the plane of shear (see Figures 2 and 3). Figures 7–10 identify the Bragg reflections associated with each system along with the indexed portions of the two-dimensional SAXS patterns.

Figure 7 highlights diffraction associated with the $\{110\}\langle\bar{1}11\rangle$ slip system. Twinned crystal configurations lead to two pairs of

principal reflections associated with the $(\bar{1}10)$ and $(1\bar{1}0)$ planes, rotated by $\pm 35^\circ$ from the shear (x) direction. All of the other allowed higher order reflections lying within the resolution of the detector are also identified in this illustration: (002) , $(\bar{1}12)$, $(\bar{1}\bar{1}2)$, $(\bar{2}20)$, $(\bar{2}22)$, $(2\bar{2}\bar{2})$. [Note, unless stated otherwise, equivalent (hkl) planes are omitted from listings that include $(\bar{h}\bar{k}\bar{l})$.] Obviously, this twinned crystal arrangement fails to account for many of the experimentally generated diffraction peaks.

Figure 8 identifies scattering attributable to the $\{211\}\langle\bar{1}11\rangle$ slip system, which contains a single slip plane (i.e., no twinning, see Figure 2). This arrangement captures the remaining leading order reflections, $(0\bar{1}1)$ [and $(01\bar{1})$], along with $(02\bar{2})$, $(\bar{2}2\bar{2})$, and $(\bar{2}13)$. Two more sets of peaks, $(\bar{1}21)$ and $(1\bar{3}0)$, associated with twinned crystals in the $\{321\}\langle\bar{1}11\rangle$ slip system, are located in Figure 9. The last four experimentally resolved diffraction spots are assigned to planes perpendicular to the slip planes in twinned versions of the $\{431\}\langle\bar{1}11\rangle$ slip system, $(\bar{0}31)$ and $(\bar{2}31)$, as shown in Figure 10. As far as we can discern, this last slip system has not been previously invoked in a block copolymer-based BCC system, presumably because previous studies have not resolved as many higher order reflections. The first three systems have been invoked in the related work of Hamley et al.¹¹ Two studies on triblock systems suggested the possibility of $\{001\}\langle 110 \rangle$ and $\{111\}\langle 211 \rangle$ slip systems,^{17,19} but as the authors noted the limited number of reflections could also be consistent with the first three systems considered here.

These diffraction assignments lead to an unanticipated yet inescapable conclusion: Dynamically shearing the weakly ordered BCC materials produces a polycrystalline texture in which each grain is oriented with one of four slip planes parallel to the shear plane and with the $\langle\bar{1}11\rangle$ direction coincident with the shear direction, as illustrated in Figure 11.

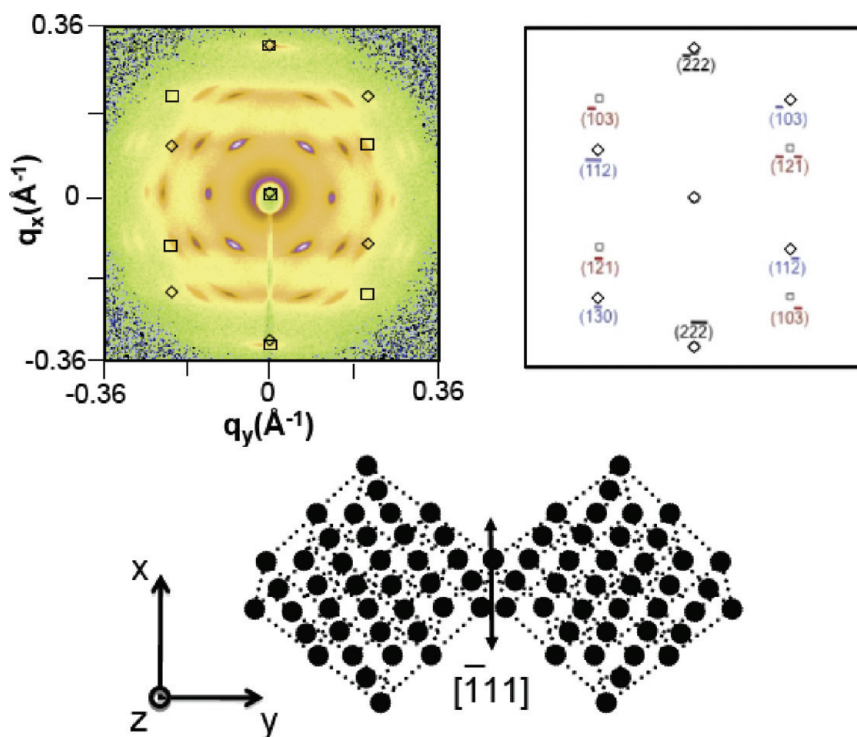


Figure 9. Identification of diffraction peaks associated with the $\{321\}\langle\bar{1}11\rangle$ slip system, where the slip plane is parallel to the plane of shear ($x-y$) and the slip direction coincides with the shear direction (x). Equivalent twinned crystal structures are shown in projection, and the associated reflections are located on the SAXS pattern using square and triangular symbols and indexed in the complementary map.

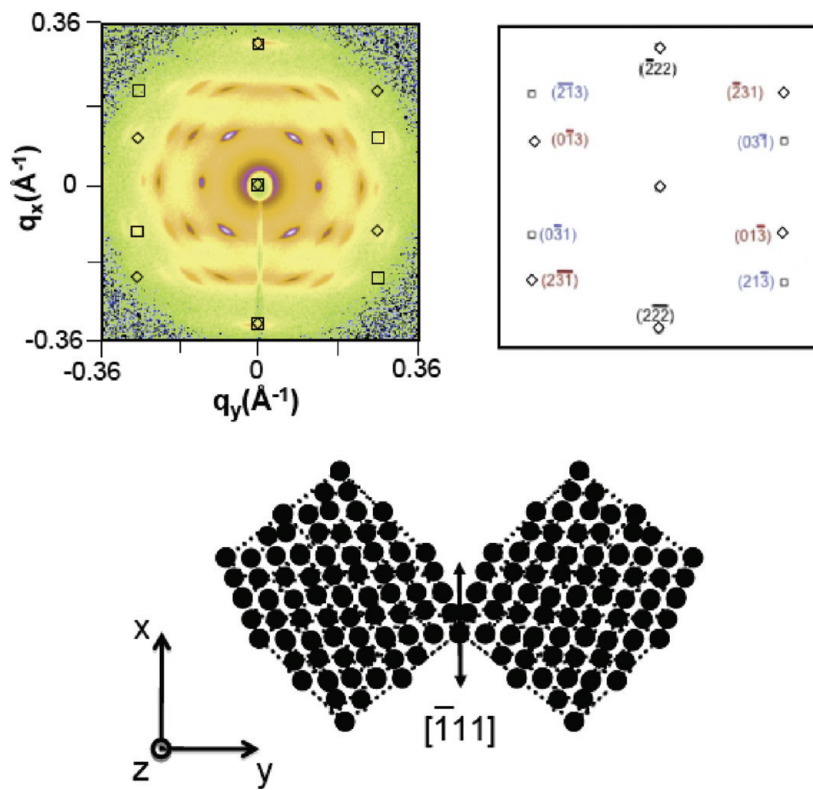


Figure 10. Identification of diffraction peaks associated with the $\{431\}\langle\bar{1}11\rangle$ slip system, where the slip plane is parallel to the plane of shear ($x-y$) and the slip direction coincides with the shear direction (x). Equivalent twinned crystal structures are shown in projection, and the associated reflections are located on the SAXS pattern using square and triangular symbols and indexed in the complementary map.

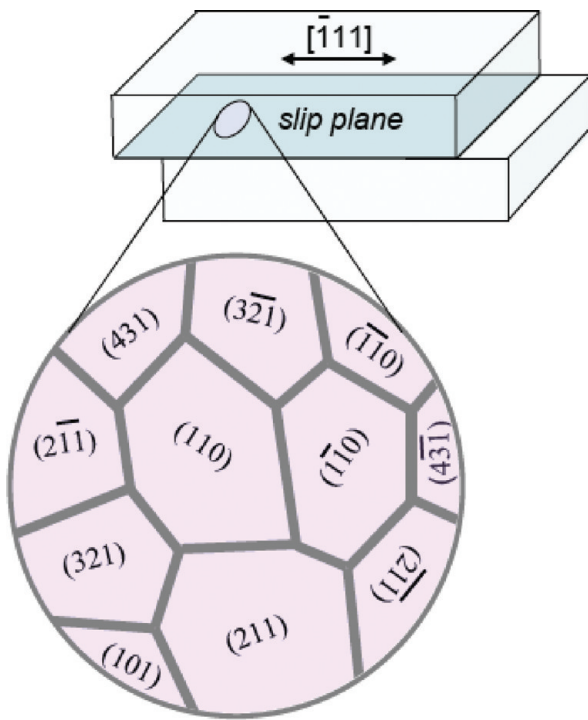


Figure 11. Schematic illustration of the polycrystalline texture produced by large amplitude oscillatory shearing of the 10% by weight mixture of SEP(42–60) in squalane. Nonlinear shearing transforms an initially isotropic distribution of crystal grains into a set of discretely oriented domains characterized by four slip systems, where the slip plane is parallel to the plane of shear and the slip direction coincides with the shear direction. This finding can be rationalized on the basis of dislocation-mediated plastic deformation analogous to the well-established behavior of ductile metals.

IV. DISCUSSION

Sphere-forming block copolymers are capable of self-assembling into a surprisingly rich array of ordered states. Conventional self-consistent mean-field theory (SCFT) anticipates BCC symmetry for diblock copolymer melts,²⁶ a prediction supported by most experimental studies. However, discovery of the σ -phase in a sphere forming poly(isoprene-*b*-lactide) (PI-PLA) diblock copolymer near the order-disorder transition²⁷ suggests a more robust compliment of equilibrium sphere-based phases in the limit of finite molecular weight. Introduction of a third block type, and more complex linear and branched architectures such as the ABAC tetrablock,²⁸ ABABAC hexablock,²⁹ and ABC star³⁰ geometries, can produce yet greater phase complexity even with the restriction of a spherical microdomain motif. Addition of diluents introduces an additional thermodynamic degree of freedom, and numerous studies have documented BCC, FCC, and HCP packing of spherical micelles in selective solvents and have shown how shearing flows can generate single crystalline (and twinned) morphologies.³¹

The results reported in this work deal with the most prevalent and best understood packing symmetry, but at a sphere density that approaches the order-disorder transition concentration. In this limit, the spherical cores constitute just 3% of the sample volume and the corona blocks are highly solvated and only weakly entangled. The interaction potential that positions the SEP(42–60) micelles on a cubic lattice is extraordinarily weak as

reflected by the elastic modulus: $G' \approx (2\text{--}3) \times 10^2$ Pa. For comparison, BCC iron is characterized by a shear modulus $G_{Fe} = 8 \times 10^{10}$ Pa.²

Stretching or shearing a metal beyond the yield point generates dislocations (initiated at impurities and grain boundaries) and activates dislocation motion, thereby facilitating slip and macroscopic plastic deformation.¹ Strained polycrystalline metals generally retain the initial grain texture when plastically deformed, accompanied by approximately affine distortion of individual crystalline domains (i.e., stretching and rotation proportional to the macroscopic sample deformation) facilitated by grain boundary sliding and slip propagation across grains.² Although the results summarized in Figures 7–10 implicate the same slip systems known to govern plasticity in BCC metals,² the mechanisms responsible for transforming the initially polydomain SEP(42–60)/squalane specimen into a collection of discretely oriented grains (see Figure 11) must involve more than simple slip. Here, we speculate on possible explanations for this outcome, while acknowledging the strikingly similar dynamic behavior of BCC metals and highly solvated yet ordered block copolymer micelles.

Even though we are not able to image dislocations in the soft block copolymer based solid, the evidence presented in Figures 7–10 is consistent with the presence of such defects in this material. An initially polycrystalline morphology (see Figure 4), with an abundance of grain boundary defects, should provide ample sources for the generation of dislocations. Dislocations contain an elastic energy per unit length given by $\epsilon \approx Gb^2$ where b is the magnitude of the Burgers vector ($b = (3)^{1/2}a/2$ for BCC crystals) and G is the shear modulus.² For the BCC SEP(42–60)/squalane system, $b \approx 60$ nm yielding $\epsilon \approx 10^{-12}$ J/m (for BCC iron, $b = 0.25$ nm and $\epsilon_{Fe} \approx 5 \times 10^{-9}$ J/m).² The mechanically stiff device employed in the dynamic shearing experiments delivers a large amplitude sinusoidal strain independent of the associated (relatively weak) stresses, which must be dissipated in the sample. A reasonable conjecture is that these strains generate dislocations. Because of the associated low energy of formation, we would not expect the associated strain energy to result in a perceptible change in sample temperature.

Because the block copolymer concentration is relatively close to the order-disorder concentration, the accumulation of dislocations could lead to melting. A sizable literature treats the topic of dislocation-induced melting in a host of materials, ranging from iron in the earth's core³² to two-dimensional hexatic liquid crystals.³³ However, if the entire block copolymer specimen melted during oscillatory shearing, there would be no evidence of grain orientation upon recrystallization after cessation of flow, contrary to what we observe experimentally (see Figure 6). Therefore, we propose that local melting facilitates grain rotation, leading to an ensemble of oriented crystals each arranged with a favorable slip system aligned with the slip plane parallel to the plane of shear and the Burgers vector coincident with the direction of shear. Once the polycrystalline specimen becomes completely oriented in this manner, strain can be accommodated by dislocation movement throughout the material. Alternatively, a narrow band of material may melt, thereby relieving local stress, with recrystallization driving propagation of the melted zone across the entire specimen. A ductile metal generally does not respond in this manner due to an elevated melting temperature and the high energy associated with dislocation formation.

We must emphasize that our hypothesis regarding slip in the block copolymer solution relies on the analogy with plastic deformation in metals. Coherent slipping of entire planes of micelles in a crystalline grain cannot be ruled out, although simple calculations (drawn directly from arguments used to rationalize the behavior of metals)² suggest this would require dramatically more strain energy than is necessary to move a dislocation. Also, the fact that the results obtained when shearing diblock micelle crystals¹¹ (sometimes misleadingly termed “gels”) and triblock gels^{17,19} are consistent argues strongly against large scale slip of neighboring planes, as the individual micelles in the triblock case are surely connected to one another through multiple bridging midblocks.

Evidence that supports our hypothesis of partial melting and grain reorientation exists in the colloidal crystal literature. Colloid particles are generally larger than block copolymer micelles and more easily imaged. Imhof et al. have shown how colloidal crystals of silica (200 nm radius) partially melt under shearing flows above a critical value.³⁴ Polarized optical microscopy reveals regions of colloidal crystal separated by bands of melted and disordered dispersion, where the extent of crystallinity is proportional to the shear rate. Although these authors did not invoke the slip arguments advanced here to rationalize the behavior of the colloidal crystals, their findings substantiate our speculated mechanism.

Even bulk metals may exhibit grain rotation during deformation in the nanocrystalline limit. Theoretical calculations³⁵ and molecular dynamics simulations³⁶ have anticipated that grain rotation may accompany grain growth in finely textured aluminum, copper, nickel, and certain alloys. Recent electron microscopy images and electron diffraction patterns obtained from nanocrystalline Ni (average grain size of 20 nm) reveal grain rotation upon straining, leading to coarsening and accompanied by crystal alignment.^{37,38} This mechanism resembles the one we have proposed to explain the shear-induced orientation of the BCC ordered grains in the block copolymer micelle system (see Figure 11). While there are significant differences between the experiments performed with the soft micelle-based crystals and the nanocrystalline metals, including different modes of deformation (reciprocating shear versus tensile strain), both systems are likely governed by a high density of defects. In nanocrystalline metals, small grain sizes produce copious amounts of grain boundaries and relatively mobile defect structures including dislocations. Conversely, the soft block copolymer micelles are arranged on an extraordinarily weak lattice that is subject to facile deformation under the effects of large amplitude forced oscillatory shear strain. As evidenced by Figures 6–10, the polycrystalline BCC material responds to this deformation by rearranging the grain structure so as to facilitate slip throughout the specimen. We believe these dynamical processes are mediated through dislocation movement, by analogy with the documented plastic behavior of metals. However, in the absence of direct images of such defects, we cannot rule out other possibilities.

Finally, the facile grain reorganization documented in this work helps explain the remarkable complete nanoscale mixing of ordered micelles that we recently reported.²³ The apparatus employed in that study imposed a complex combination of shearing and extensional flows on initially macroscopic pieces of normal and deuterium labeled BCC crystals. On the basis of the results reported here, this mixing action will produce massive slip along a multitude of directions, together with constant folding and recombining of the material. Clearly, these flow

patterns, combined with extensive dislocation mediated slip, will quickly randomize the placement of labeled and unlabeled micelles throughout the specimen. We will explore the shear rate and strain amplitude dependence of this grain rotation effect in a future publication.

■ AUTHOR INFORMATION

Corresponding Author

*E-mail: bates@cem.s.umn.edu (F.S.B.); lodge@umn.edu (T.P.L.).

■ ACKNOWLEDGMENT

This work was supported by the MRSEC program of the National Science Foundation, through Award DMR-0819885, by Infineum USA, L. P., and by the College of Science and Engineering Characterization Facility.

■ REFERENCES

- (1) Weertman, J.; Weertman, J. R. *Elementary Dislocation Theory*; Macmillan: New York, 1964 (reprinted by Oxford University Press: New York, 1992).
- (2) Barrett, C. R.; Nix, W. D.; Tetelman, A. S. *The Principles of Engineering Materials*; Prentice-Hall: Englewood Cliffs, NJ, 1973.
- (3) Bates, F. S.; Fredrickson, G. H. *Phys. Today* **1999**, *52*, 32.
- (4) Keller, A.; Odell, A. *Nature* **1970**, *225*, 538.
- (5) Almdal, K.; Koppi, K. A.; Bates, F. S. *Macromolecules* **1993**, *26*, 4058.
- (6) Koppi, K. A.; *J. Rheol.* **1994**, *38*, 999.
- (7) Park, M.-J.; Bang, J.; Harada, T.; Char, K.; Lodge, T. P. *Macromolecules* **2004**, *37*, 9064–9075.
- (8) Okamoto, S.; Saijo, K.; Hashimoto, T. *Macromolecules* **1994**, *27*, 3753–3758.
- (9) McConnell, G. A.; Lin, M. Y.; Gast, A. P. *Macromolecules* **1995**, *28*, 6754–6764.
- (10) Hamley, I. W.; Pople, J. A.; Fairclough, J. P. A.; Terrill, N. J.; Ryan, A. J.; Booth, C.; Yu, G.-E.; Diat, O.; Almdal, K.; Mortensen, K.; Vigild, M. *J. Chem. Phys.* **1998**, *108*, 6929.
- (11) Hamley, I. W.; Pople, J. A.; Booth, C.; Yang, Y.-W.; King, S. M. *Langmuir* **1998**, *14*, 3182–3186.
- (12) Shin, G.; Sakamoto, N.; Saijo, K.; Suehiro, S.; Hashimoto, T.; Ito, K.; Amemiya, Y. *Macromolecules* **2000**, *33*, 9002–9014.
- (13) Watanabe, H.; Matsumiya, Y.; Kanaya, T.; Takahashi, Y. *Macromolecules* **2001**, *34*, 6742–6755.
- (14) Sebastian, J. M.; Lai, C.; Graessley, W. W.; Register, R. A.; Marchand, G. R. *Macromolecules* **2002**, *35*, 2700–2706.
- (15) Sebastian, J. M.; Lai, C.; Graessley, W. W.; Register, R. A. *Macromolecules* **2002**, *35*, 2707–2713.
- (16) Sebastian, J. M.; Graessley, W. W.; Register, R. A. *J. Rheol.* **2002**, *46*, 863–879.
- (17) Mortensen, K.; Theunissen, E.; Kleppinger, R.; Almdal, K.; Reynaers, H. *Macromolecules* **2002**, *35*, 7773–7781.
- (18) Habas, J.-P.; Pavie, E.; Perreux, C.; Lapp, A.; Peyrelasse, J. *Phys. Rev. E* **2004**, *70*, 061802.
- (19) Mandare, P.; Winter, H. H. *Rheol. Acta* **2007**, *46*, 1161–1170.
- (20) Choi, S.; Bates, F. S.; Lodge, T. P. *J. Phys. Chem. B* **2009**, *113*, 13840–13848.
- (21) Choi, S.; Lodge, T. P.; Bates, F. S. *Phys. Rev. Lett.* **2010**, *104*, 047802.
- (22) Choi, S.; Bates, F. S.; Lodge, T. P., submitted.
- (23) Choi, S.; Lee, S.; Soto, H.; Lodge, T. P.; Bates, F. S. *J. Am. Chem. Soc.* **2011**, *133*, 1722–1725.
- (24) Wang, C.-Y.; Lodge, T. P. *Macromol. Rapid Commun.* **2001**, *23*, 49.
- (25) Kossuth, M. B.; Morse, D. C.; Bates, F. S. *J. Rheol.* **1999**, *43*, 167–196.
- (26) Leibler, L. *Macromolecules* **1980**, *13*, 1602–1617.

- (27) Lee, S.; Bluemle, M. J.; Bates, F. S. *Science* **2010**, *340*, 349–353.
- (28) Bluemle, M. J.; Fleury, G.; Lodge, T. P.; Bates, F. S. *Soft Matter* **2009**, *5*, 1587–1590.
- (29) Fleury, G.; Bates, F. S. *Macromolecules* **2009**, *42*, 1691–1694.
- (30) Hayashida, K.; Dotera, T.; Takano, A.; Matsushita, Y. *Phys. Rev. Lett.* **2007**, *98*, 195502.
- (31) Bang, J.; Lodge, T. P. *J. Phys. Chem. B* **2003**, *107*, 12071–12081.
- (32) Poirier, J. P.; Price, G. D. *Phys. Earth Planet. Inter.* **1992**, *69*, 153–162.
- (33) Chou, C. F.; *Science* **1998**, *280*, 1424–1426.
- (34) Imhof, A.; van Blaaderen, A.; Dhont, J. K. G. *Langmuir* **1994**, *10*, 3477–3484.
- (35) Moldovan, D.; Yamakov, V.; Wolf, D.; Phillpot, S. R. *Phys. Rev. Lett.* **2002**, *89*, 206101.
- (36) Van Swygenhoven, H.; Derlet, P. M.; Hasbaoui, A. *Adv. Eng. Mater.* **2003**, *5*, 345–350.
- (37) Shan, Z.; *Science* **2004**, *305*, 654–657.
- (38) Wang, Y. B.; Li, B. Q.; Sui, M. L.; Mao, S. X. *Appl. Phys. Lett.* **2008**, *92*, 011903.